

1
2
3
4
5
6
7
8
9
10
11
12
13
14
15
16
17
18
19
20
21
22
23
24
25
26
27
28
29
30
31

Anonymous Referee #1

We express our gratitude to Referee for the valuable comments and remarks.

1. C. The paper relay heavily on the theoretical work presented in Pinsky 2012 and previous works. It would be nice to have this paper on a more “standalone mode”. A summary of the main assumptions and derivations would make it much useful.

(R) We added more details in description of the approach in Section 2 (model description). A short derivation of the basic equation for supersaturation maximum is presented in new Appendix.

2. C. On the same note, throughout the paper the validation of the new scheme (NA) should be better explained. When the results are compared to a one D model – is it a parcel model? When the authors state that the results of the NA are “much better” they should explain more on how they reached this conclusion.

(R) We used the parcel model to calculate supersaturation maximum and concentration using CCN distribution and vertical velocity at the cloud base as in the HUCM simulations. New Fig 2 shows that New Approach produces the values of supersaturation and droplet concentrations much closer to "exact" values obtained by the parcel model than to the values obtained in ST.

3. (C) Does the model with the new scheme assigns S_{max} as the supersaturation for all of the gridbox near cloud base? If yes wouldn't it results in an overestimation of the activation? If not please explain why?

(R) The values of S_{max} are calculated at all grid points that we assume to be associated to cloud base (the first grid point from below at which $S_w \geq 0$). Some overestimation is possible in case of very high concentration as it is shown by Pinsky et al. (2012), but this error is substantially lower than in case Standard Approach is used.

4) (C) Is this parameterization done only for the gridbox near (above) cloud base? If yes how does the LCL is found? How sensitive is it to the location of the theoretical LCL within the gridbox? Say that in one

32 case the theoretical LCL is toward the upper part of the gridbox, wouldn't it make more sense to assign
33 the Smax parameter to the gridbox above? How sensitive it is to such details?

34
35 (R) We determine the model cloud base in the way described in the response above. In this
36 approach, the grid point is slightly above the theoretical LCL, because we use condition $S_w \geq 0$. At the
37 same time, the calculations performed according to Pinsky et al. (2012) show that the level where
38 $S_w = S_{max}$ is located, i.e. from about 20 m (for high CCN concentration) to about 60 m (for low CCM
39 concentration) is higher than the LCL. The estimations show, therefore, that the level where $S_w = S_{max}$ is
40 quite close to the model cloud base level. Accordingly, the droplet concentration determined at
41 $S_w = S_{max}$ is assigned to the corresponding grid point at the model cloud base. We believe that the fact
42 that we assign the droplet concentration calculated at the point of Smax to the lower model level, where
43 $S_w \geq 0$, does not lead to serious errors.

44
45 5) (C) Smax and N (number of activated droplets) are coupled. Smax depends on N and N (or r(critical
46 for activation)) on Smax. Could the authors explain how they solve them both and it the analytical
47 parametrization? I guess one equation is eq. 3 but another equation is needed.

48
49 (R) Detailed explanations are added in Section 2.

50
51

52 **Anonymous Referee #2**

53 We express deep gratitude to Referee for the valuable comments and remarks.

54 1) The Introduction is short and sounds incomplete. It can be expanded to include (1) the importance of
55 droplet nucleation to cloud properties and precipitation, (2) the description of the current approach (ST)
56 and its limitation.

57
58 (R) The introduction is rewritten in more detail. It is stressed that droplet concentration determines
59 major microphysical cloud properties such as height of precipitation onset, type of precipitation (liquid,
60 mixed phase and ice). The description of Standard Approach is given, its limitations are mentioned. The
61 necessity of exact calculation of cloud droplet concentration at cloud base is stressed.

62 New Approach is described in more detail in Section 2. A new Appendix is added to describe the
63 derivation of the basic equation for supersaturation maximum.

64

65 C. If the authors want to claim that the NA method gives more realistic droplet nucleation than
66 ST and also to better evaluate both the ST and NA, it is necessary to conduct a benchmark test in
67 which very high vertical resolution is used to resolve the maximum supersaturation and compare the
68 supersaturation and droplet concentration with those from the benchmark test. In addition, the
69 authors have a statement that the NA can be applied to any vertical resolution. By comparing S_{max}
70 parameterized with the model predicted in such a test can help support that conclusion as well. This
71 test should not be difficult to do with the idealized 2-D model.

72

73 (R) We conducted the benchmark test. The values of supersaturation and droplet concentrations in the
74 vicinity of cloud base calculated using ST and NA were compared with supersaturation and droplet
75 concentration calculated using a high precision parcel model. It is shown that results obtained using NA are
76 much closer than ST results to those obtained by means of the parcel model.. This comparison is presented
77 in new Fig. 2.

78

79 3.(C) Some clarification is needed for the description of NA method (Section 2)

80

81 (R) the description of NA is clarified. The derivation of the equations is presented in new Appendix.

82 (C) Additional discussion is needed throughout Section 4 (see the specific comments below).

83 (R). The discussion is added (see responses to the specific questions).

84 Specific comments:

85 1) Line 134-139, for Eq (3), I am confused here, how did you solve three unknowns (S_{max} , the critical
86 radius of the aerosols activated, and the nucleated droplet concentration) with Eq. 3?

87

88 (R). The detailed explanation is presented in Section 2.

89

90 2) (C) Line 142, what is the new microphysical scheme? A little more details are needed here.

91 (R) The new microphysical scheme is NA described in the model description section.

92 The sentence was changed as follows:

93 Effects of NA on cloud microphysics were tested...

94

95

96

97 3) C. Line 147-151, do you mean the simulation is not initiated with a real sounding? Then I would like to
98 see some justifications how the used dynamics and thermodynamics are close to a realistic atmosphere
99 condition.

100
101
102
103
104
105
106
107
108
109
110
111
112
113
114
115
116
117
118
119
120
121
122
123
124
125
126
127
128
129
130
131
132
133
134
135
136
137
138
139

(R) We use the surface temperature during the storm pass. To avoid confusion, the sentence was deleted.

4) Line 161-162 and Line 167-168, for the clean conditions, why the minimum CCN radius is set to be a little smaller than the polluted conditions?

(R) According to Ghan et al. (2011, Table 2) the nuclei mode (the smallest CCN) in Marine aerosol size distribution contains aerosols smaller than the nuclei mode in Continental case or even than in Urban case. This comment is included into the revised paper.

5) (C) Line 196-200, Figure 2 does not show the results of Sw and droplet concentrations. Please present the results.

(R) New Fig. 2 is presented in the revised version.

6) C. Line 253-256, the statement about “the decrease in the snow mass content” in the more droplet nucleation condition is not what Fig. 6 shows. Snow water content in EN3500-S is lower than E3500-S. Also, the NA method produces such greater graupel water content than the ST when shape parameter is 0.9. Is this related to a certain threshold used in the C2 ACPD Interactive comment Printer-friendly version Discussion paper riming processes to form graupel? In the tests with the shape factor of 0.5, the increase is not as dramatic. Why?

(R) The text is rewritten in a clearer manner. Snow water mass content in EN3500-S is lower than E3500-S because riming is more efficient in EN3500-S as compared to E3500-S (more supercooled water was nucleation at cloud base and ascent to higher levels increase the riming). The rimed snow is converted to graupel. This also explains the increase in mass content of graupel and hail in all NA cases. The difference in supercolled water is less pronounced when at slope parameter $k=0.5$ (see Fig. 4). The existence of the smallest CCN concentration (at $k=0.9$) leads to an increase in the differences between NA and ST. We attribute this difference to the fact that in E3500-S the liquid water content at upper levels is higher, which leads to larger graupel mass formed by riming.

7) C. Figure 8 and Line 272-276, the discussion here should be compared with Figure 4 which shows that results for the high CCN condition. The differences between NA and ST in droplet number concentration are smaller, which is limited by available CCN. Also, CWC peaks at very different height compared with the high CCN condition.

The comparison is added. The differences between the cases plotted in Fig 4 and 8 are discussed in detail.

140 8) Figure 9 and Line 297-298, the statement is not right about hail. The hail mass content is the largest in
141 the E100 and EN100 where no smaller CCN exist and droplet concentration is the lower than others. In
142 addition, please discuss such high sensitivity of graupel to the small CCN (i.e. droplet number concentration
143 under the maritime cloud condition and give possible reasons about it.

144 (R) Done. The text is rewritten as follows:

145
146 The mass content of snow decreases with the increase in the smallest CCN concentration, because the
147 smallest CCN increase supercooled drop content that leads to intensification of riming of snow. In turn,
148 riming leads to its conversion to graupel (Fig. 9b). Consequently, the graupel mass content increases (Fig. 9c).
149 As regards to mass content of hail, the increase in the the smallest CCN concentration leads to a decrease in
150 the hail content above 6 km and to its increase below this level (Fig. 9d). The higher hail mass content
151 above 6 km layer in the absence of smallest CCN is likely related to the fact the low droplet concentration
152 leads to formation of raindrops in high concentration. Although these raindrops are of comparatively small
153 size, the total raindrop mass content is larger than that in case of higher drop concentration. These
154 raindrops rapidly freeze above the freezing level producing hail (actually frozen drops) with total mass larger
155 than at high CCN concentration. This effect is discussed by Ilotovich et al. (2016) in detail. In HUCM, frozen
156 raindrops are assigned to the hail category due to their high density. If hail is defined as particles with sizes
157 exceeding 1 cm, the amount of hail at low CCN concentration would be negligible.

158 Higher hail mass content below 6 km in the presence of the smallest CCN can be attributed to intense
159 conversion of heavy rimed graupel to hail, as well as to more efficient hail growth by riming. In a deep
160 convective cloud developing in the polluted atmosphere more hail particles from as compared to a cloud
161 developing in clean air (Ilotovich et al. 2016). Due to larger size, hail in the polluted case falls to the surface
162 (Fig. 6d), while in clean air hail melts at 1.5 km in the absence of no small CCN and in vicinity of the surface in
163 case if the CCN size spectrum contains the smallest CCN.

164
165
166 9) C. Figure 10d and line 315-319, why does the hail precipitation in EN100-S-0.5 is much less than E100-
167 S-0.5 since effect of small CCN is also included in this set of tests?

168 Amount of hail at the surface in polluted air (Figure 10c) is substantially larger than in clean air s (Figure
169 10d) due to lower sizes and faster melting of hail particles at low CCN concentration. The effect of AP on
170 the size and amount of hail at the surface was investigated by Ilotovich et al. (2016) in detail.

171 The main factor determining the differences in the amount of hail falling to the surface in cases of low
172 CCN concentration is effect of smallest CCN. The increase in concentration of smallest CCN leads to an
173 increase in hail growth by riming.

174
175 As regards to the ratios of hail amounts in each group (with high and small CCN concentrations), for
176 instance in the simulations EN100-S-0.5 and E100-S-0.5, these ratios change because of the earlier or later
177 intensification of convective cells. Since the mass of hail falling to the surface (especially in clean air) is very
178 low, a larger computational area is required to obtain reliable statistics and to get certain conclusions. Since
179 at times exceeding about 200 min simulated cloud approached the lateral boundary, we re-plotted figure
180 10, so the time dependencies are shown till 180 min (instead of 220 min in the earlier version).

181

182 10) Line 345-347, I do not understand this statement, the small CCN increase droplet concentrations at
183 the much higher levels, not around cloud base, how can it be made up by using the NA method? I did not
184 see such results from Figures 4 and 8. I think the conclusion should be in-cloud nucleation has to be
185 considered in the case of existing small CCN.

186 (R) The error in the calculation of the droplet concentration near cloud base in ST is compensated to a
187 significant extent by in-cloud nucleation above cloud base. Indeed, in NA droplet concentration increases
188 with height up to the level of 4 km (Fig. 4a). The only reason of such increase is the in-cloud nucleation of
189 comparatively large CCN. Smallest CCN are activated at higher levels. Corresponding comments are included
190 into the revised paper.

191 11) C. Line 366-368, see my comment in #8.

192 (R) The effect of the smallest CCN on hail is discussed in the body of the paper. The sentence pointed out
193 by Referee is changed to:

194 "The smallest CCN also influence hail size and mass content".

195 12)C. Line 382-383, the statement "It can be used in cloud-resolved models with different vertical grid
196 spacing", is not supported by the content yet. By adding the benchmark test in which Smax calculated with
197 NA can be compared with the model predicted Smax would address this problem.

198
199 (R). The comparison with the benchmark parcel model is included and discussed.

200

201 **References:**

202

203 Ilotoviz, E., A. Khain, N. Benmoshe, V. T. J. Phillips, and A. Ryzhkov, 2016: Effect of aerosols on freezing
204 drops, hail and precipitation in a mid-latitude storm. *J. Atmos. Sci.*, **73**, 109-144,
205 <http://dx.doi.org/10.1175/JAS-D-14-0155.1>.

206 Khain, A. P., BenMoshe, N. and A. Pokrovsky: Factors Determining the Impact of Aerosols on
207 Surface Precipitation from Clouds: An Attempt at Classification, *J. Atmos. Sci.*, **65**(6), 1721–1748,
208 doi:10.1175/2007JAS2515.1, 2008.

209 Khain, A. P., Phillips, V., Benmoshe, N. and A. Pokrovsky: The Role of Small Soluble Aerosols
210 in the Microphysics of Deep Maritime Clouds, *J. Atmos. Sci.*, **69**(9), 2787–2807,
211 doi:10.1175/2011JAS3649.1, 2012.

212 Pinsky, M., Khain, A., Mazin, I. and Korolev, A.: Analytical estimation of droplet concentration
213 at cloud base, *J. Geophys. Res. Atmos.*, **117**(D18), n/a–n/a, doi:10.1029/2012JD017753, 2012.

214

215
216
217
218
219
220
221
222
223
224
225
226
227
228
229
230
231

**Application of a new scheme of cloud base droplet nucleation in a
Spectral (bin) Microphysics cloud model: sensitivity to aerosol size
distribution**

E. Ilotoviz and A. Khain

Department of Atmospheric Sciences, The Hebrew University of Jerusalem, Israel

Submitted to Atmos. Chem. Phys. Discuss.

June 2016

Revised

21 September 2016

Communicating author: Alexander Khain, Department of Atmospheric Sciences, The Hebrew
University of Jerusalem, Israel, email: alexander.khain@mail.huji.ac.il

232 **Abstract**

233 A new scheme of droplet nucleation at cloud base is implemented into the Hebrew University
234 Cloud Model (HUCM) with spectral (bin) microphysics. In this scheme, supersaturation
235 maximum S_{max} near cloud base is calculated using theoretical results according to which
236 $S_{max} \sim w^{3/4} N_d^{-1/2}$, where w is the vertical velocity at cloud base and N_d is droplet concentration.
237 Microphysical cloud structure obtained in the simulations of a mid-latitude hail storm using the
238 new scheme is compared with that obtained in the standard approach, in which droplet nucleation
239 is calculated using supersaturation calculated in grid points. The simulations were performed
240 with different concentrations of cloud condensational nuclei (CCN) and with different shapes of
241 CCN size spectra. It is shown that the new nucleation scheme substantially improves the vertical
242 profile of droplet concentration shifting the concentration maximum to cloud base. It is shown
243 that the effect of the CCN size distribution shape on cloud microphysics is not less important
244 than the effect of the total CCN concentration. It is shown that the smallest CCN with diameters
245 less than about $0.015 \mu m$ have a substantial effect on mixed-phase and ice microphysics of deep
246 convective clouds. Such CCN are not measured by standard CCN probes which hinders
247 understanding of cold microphysical processes.

248

249 Key words: cloud-aerosol interaction, droplet nucleation at cloud base, spectral bin
250 microphysics

251

252

253

254

255 **1. Introduction**

256 Droplet concentration is the key microphysical parameter that affects precipitation formation,
257 and radiative cloud properties (Pruppacher and Klett, 1997). The droplet concentration determines
258 major microphysical cloud properties such as height of precipitation onset, type of precipitation
259 (liquid, mixed phase and ice) (Khain, 2009; Freud and Rosenfeld, 2012; Tao et al. 2012) . Droplet
260 concentration is determined by concentration and size distribution of aerosol particles (AP) and by
261 the maximum value of supersaturation near cloud base S_{\max} . S_{\max} is reached at a few tens of
262 meters above cloud base (Rogers and Yau, 1996). The vertical grid spacing of most cloud-
263 resolving models is too coarse to resolve this maximum. This can lead to errors in determination
264 of droplet concentration. Therefore, it is desirable to parameterize the process of droplet
265 nucleation near cloud base. One approach to the parameterization is based on lookup tables
266 developed using precise 1D parcel models (e.g., Segal and Khain, 2006). The other approach is
267 based on analytical calculation of supersaturation maximum, S_{\max} , near cloud base. This approach
268 has been developed in several studies using various assumptions concerning CCN activity spectra
269 (Ghan et al., 1993, 1997; Bedos et al., 1996; Abdul-Razzak et al., 1998; Cohard et al., 1998;
270 Abdul-Razzak and Ghan, 2000; Fountoukis, 2005; Shipway and Abel, 2010). In these studies
271 calculation of a supersaturation maximum is reduced to solving a complicated integro-differential
272 equation assuming different expressions for CCN activation spectra. The parameters of activation
273 CCN spectra, as well as the concentration and shape of the CCN size distributions, are often
274 prescribed in atmospheric models and assumed to be invariant over time. The results and a
275 comparison of these approaches are presented by Ghan et al. (2011).

276 In cloud models with a comparatively high resolution (Kogan 2001; Khain et al. 2014)
277 supersaturation S_w is calculated explicitly at each grid point. In these bin microphysics models AP
278 playing the role of cloud condensational nuclei (CCN) are described using aerosol size distribution
279 functions containing several tens of size bins. The value of supersaturation is used to calculate the
280 critical radius of AP using the Köhler theory. All CCN with sizes exceeding this critical value are
281 activated to droplets. This approach will be referred to as standard approach (ST) where
282 supersaturation maximum near cloud base is not resolved and the vertical profile of
283 supersaturation may not contain such maximum. It leads to underestimation of droplet
284 concentration in clouds, at least in their low part.

285 In set of studies by Pinsky et al. (2012, 2013, 2014) formation of profiles of supersaturation
286 and of droplet concentration were investigated both analytically and by means of a high precision
287 model of an ascending adiabatic parcel. Pinsky et al. (2012) proposed a simple method of
288 calculating S_{\max} near cloud base for monodisperse aerosol size distribution. The detailed test
289 showed that the method can be applied to any CCN spectra. Pinsky et al (2014) gave a theoretical
290 basis for such conclusion by calculating droplet concentrations using multidisperse size spectra of
291 AP. The method of calculating droplet concentration near cloud base using S_{\max} will be referred to
292 as *new approach* (NA).

293 In this study we investigate the effects of application of NA on the microphysics of mid-
294 latitude deep convective clouds (hail storm) using the Hebrew University Cloud model (HUCM)
295 with spectral-bin microphysics (SBM). The effect of the new approach is investigated in
296 simulations with different parameters of CCN activation spectra.

297

298 **2. Model description**

299 The HUCM is a 2-D, nonhydrostatic SBM model with microphysics based on solving a
300 system of equations for size distributions of liquid drops, three types of pristine ice crystals
301 (plates, columns, and dendrites), snow/aggregates, graupel, hail and partially frozen or "freezing
302 drops". Each size distribution is discretized into 43 mass-doubling bins, with the smallest bin
303 equivalent to the mass of a liquid droplet of radius $2 \mu\text{m}$. AP playing the role of CCN are also
304 defined on a mass grid containing 43 mass bins. The size of dry CCNs ranges from $0.005 \mu\text{m}$ to 2
305 μm .

306 Primary nucleation of each ice crystal type is described using Meyers et al. [1992]
307 parameterization. The type of ice crystals is determined depending on temperature range where
308 the particles arise (Takahashi et al., 1991). Secondary ice generation is taken into account during
309 riming (Hallett and Mossop 1974). Collisions are described by solving the stochastic collection
310 equations for the corresponding size distributions using the Bott (1998) method. Height-
311 dependent, gravitational collision kernels for drop-drop and drop-graupel interactions are taken
312 from Pinsky et al. (2001) and Khain et al. (2001); those for collisions between ice crystals are
313 taken from Khain and Sednev (1995) and Khain et al. (2004). The latter studies include the
314 dependence of particle mass on the ice crystal cross-section. The effects of turbulence on
315 collisions between cloud drops are included (Benmoshe et al. 2012). The collision kernels depend
316 on the turbulence intensity and changes over time and space.

317 The time-dependent melting of snow, graupel, and hail as well as shedding of water from hail
318 follows the approach suggested by Phillips et al. (2007). We have implemented liquid water mass
319 in these hydrometeor particles that is advected and settle similarly to the mass of the
320 corresponding particles. As a result, these particles are characterized by their total mass and by the
321 mass of liquid water (i.e., the liquid water mass fraction). The liquid water fraction increases

322 during melting. As soon as it exceeds ~95%, the melting particles are converted to raindrops.
323 Process of time dependent freezing is described according to Phillips et al. (2014, 2015). The
324 freezing process consists of two stages. The first nucleation stage is described using the
325 parameterization of immersion drop freezing proposed by Vali (1994) and Bigg (1953). Drops
326 with radii below $80 \mu m$ that freeze are assigned to plates, whereas larger drops undergoing
327 freezing are assigned to freezing drops. The freezing drops consist of a core of liquid water
328 surrounded by an ice envelope. Time-dependent freezing of liquid within freezing drops is
329 calculated by solving the heat balance equations that take into account the effects of accretion of
330 supercooled drops and ice particles. Collision between freezing drops and other hydrometeors lead
331 either to the freezing drops category if the freezing drop is larger than its counterpart. Otherwise,
332 the resulting particle is assigned to the type of counterpart. Once the liquid water fraction in a
333 freezing drop becomes less than some minimal value (<1%) it is converted to a hailstone. Hail can
334 grow either by dry growth or by wet growth (Phillips et al. 2014, 2015). Accordingly, liquid water
335 is allowed in hail and graupel particles at both positive and negative temperatures. The shedding
336 of water in wet growth is also included.

337 Water accreted onto aggregates (snow) freezes immediately at temperatures below $0^{\circ}C$,
338 where it then contributes to the rimed fraction. This rimed mass distribution is advected and settle
339 similarly to the snow masses. Riming mass increases the density of the aggregates. As the bulk
340 density of snow in a certain mass bin exceeds a critical value ($0.2 g cm^{-3}$), the snow from this bin
341 is converted into graupel. The appearance of water on the surface of hailstones as well as an
342 increase in the rimed fraction of snowflakes affect the particle fall velocities and coalescence
343 efficiencies.

344 The initial size distribution of CCN (at $t=0$) is calculated using the empirical dependence (i.e.,
345 the Twomey formula) of concentration N_{ccn} of activated CCN on supersaturation S_w (in %)
346 $N_{ccn} = N_o S_w^k$, where N_o and k are the measured constants (Khain et al., 2000). The obtained
347 aerosol size distribution is corrected in zones of very small and very large CCN, that is, in size
348 ranges where the Twomey formula is invalid. At $t>0$ the prognostic equation for the size
349 distribution of non-activated CCN is solved. Using the value of S calculated at each time-step and
350 in each grid point, the critical radius of CCN particles was determined according to the Köhler
351 theory. The CCNs with radii exceeding the critical value are activated and new droplets are
352 nucleated. The corresponding bins of the CCN size distributions become empty. In ST, this
353 procedure is used at all cloud grid points.

354 In NA, droplet concentration at cloud base is calculated using the formula for S_{max} derived
355 by
356 Pinsky et al. (2012)

$$357 \quad S_{max} = C w^{3/4} N_d^{-1/2}, \quad (1)$$

358 where w is vertical velocity at cloud base, N_d is droplet concentration and coefficient C slightly
359 depends on the thermodynamical parameters only (see **Table 1** for notations). A brief derivation
360 of the formula (1) is presented in **Appendix**. Since the droplet concentration at cloud base is equal
361 to the concentration of CCN activated at $S_w = S_{max}$, the droplet concentration at the cloud base can
362 be calculated as:

$$363 \quad N_d = \int_{r_{n-cr}(S_{max})}^{\infty} f(r_n) dr_n \quad (2)$$

364 where $f(r_n)$ is a size distribution of dry AP and r_{n_cr} is critical radius of CCN activated under
 365 S_{\max} . According to the Köhler theory, the critical radius relates to S_{\max} as

$$366 \quad r_{n_cr} = \frac{A}{3} \left(\frac{4}{BS_{\max}^2} \right)^{1/3}, \quad (3)$$

367 where coefficients A and B are the coefficients of the Köhler equation for equilibrium
 368 supersaturation (see Table 1 for notations). Substituting Eq. (2) into (1) one can obtain equation
 369 for S_{\max} :

$$370 \quad S_{\max} \left[\underbrace{\int_{r_{n_cr}(S_{\max})}^{\infty} f(r_n) dr_n}_{N_d} \right]^{1/2} = Cw^{3/4} \quad (4)$$

371 Taking into account the relationship (3), Eq. (4) contains only one unknown S_{\max} . This
 372 equation is easily solved by iteration calculating S_{\max} , $r_{n_cr}(S_{\max})$ and concentration of nucleated
 373 droplets at cloud base at each time step.

374 The values of S_{\max} were calculated ~~in~~ at all grid points corresponding to cloud base, which is
 375 determined as the first grid point from below, ~~in~~ at which $S_w \geq 0$.

376

377 3. Design of simulations

378 All simulations were performed within a computational domain of 153.9 km x 19.2 km, and
 379 a grid spacing of 300 m in the horizontal direction and 100 m in the vertical direction. Effects of
 380 NA on cloud microphysics were tested in simulations of a thunderstorm observed in Villingen-
 381 Schwenningen, southwest Germany, on June 28, 2006. Meteorological conditions (including
 382 sounding) of this storm are described by Khain et al. [2011]. The background wind direction was

383 quasi-2-D, which simplified the prescription of the background wind profile in the 2-D model. The
384 wind speed increased with height from $\sim 10 \text{ m s}^{-1}$ in the lower atmosphere to about 20 m s^{-1} at
385 levels of 100-200 mb. Surface temperature was 22.9°C , the relative humidity near the ground was
386 high ($\sim 85\%$), which led to a low lifting condensation level of about 890 m. The freezing level was
387 located at around 3.5 km. The observed maximum diameter of hailstones was about 5 cm.

388 The convection was triggered by a cool pool, which is typical in simulations of long-lasting
389 convection (Rotunno and Klemp, 1985).

390 Three sets of simulations were performed, each simulation in two versions: according to ST
391 where the critical CCN radius was calculated using a supersaturation calculated at the grid points
392 using the values of temperature and humidity, and according to NA where the critical CCN radius
393 and S_{max} were determined from Eq. (9).

394 *The first set of simulations* aims at the comparison of the microphysics between NA and ST
395 in cases of high ($N_0 = 3500 \text{ cm}^{-3}$) and low ($N_0 = 100 \text{ cm}^{-3}$) CCN concentrations. Minimum
396 CCN radii were set equal to $0.015 \text{ }\mu\text{m}$ and $0.0125 \text{ }\mu\text{m}$, respectively. These values correspond to
397 the data according to which **the nuclei mode (the smallest CCN) in Marine aerosol size**
398 **distribution contains aerosols smaller than the nuclei mode in Continental case or even than in**
399 **Urban case** (Ghan et al, 2011). Similar CCN size distributions were used by Khain et al (2011).
400 These simulations are referred to as E3500, E100 (T) and EN3500, EN100 (NA), respectively.

401 *In the second set of simulations* the smallest CCN were added into the AP spectra. The large
402 impact of the smallest CCN in formation of ice crystals in cloud anvils was shown by Khain et al.
403 (2012). The minimum CCN radii were taken equal to $0.006 \text{ }\mu\text{m}$ and $0.003 \text{ }\mu\text{m}$ in cases of high
404 and low CCN concentrations, respectively. These simulations are referred to as E3500-S, EN3500-
405 S, E100-S and EN100-S, where symbol "S" denotes small AP.

406 In the first and the second sets of simulations the slope parameter k was assumed equal to 0.9.
407 *The third set of simulations* was similar to the second one, but with the slope parameter k
408 $=0.5$. In many studies investigating effects of aerosols on cloud microphysics only parameter N_0
409 is changed. However, the slope parameter determines the relationship between concentration of
410 smaller and larger CCN, so concentration of nucleated droplets also depends on the slope
411 parameter. The simulations of the third set are referred to as E3500-S-05, EN3500-S-05, E100-S-
412 05 and EN100-S-05. Size distributions of CCN in the simulations are shown in **Figure 1**.

413 CCN concentrations in the simulations are presented in **Table 2**. Although the difference
414 between the total aerosol concentrations is not large, in case $k=0.5$ the CCN size distribution
415 contains more large CCN and fewer small CCN. These size distributions were assumed within the
416 lower 2-km layer. Above this level, the CCN concentration in each mass bin was decreased
417 exponentially with height. **Above 8 km, the CCN concentration was set constant.**

418

419 **4. Results of simulations**

420

421 **4.1 Vertical profiles of supersaturation near cloud base**

422 The model calculates supersaturation at the model grid points which typically do not
423 exactly coincide with the cloud base level where supersaturation $S_w=0$. We consider the first level
424 where $S_w \geq 0$ as the cloud base. Since the supersaturation maximum is reached not far from the
425 cloud base level, especially for high AP concentration cases (Pinsky et al. 2012), we attribute the
426 values of S_{\max} to this level. Correspondingly, the difference between NA and ST in the droplet
427 concentrations is also attributed to this level. **Figure 2** shows vertical profiles of supersaturation
428 calculated in ST and NA simulations in the atmospheric columns where the velocity at cloud base

429 was equal to 1 ms^{-1} . It is natural that the values of S_{max} are larger in case of low CCN
430 concentration as compared to high CCN concentration case. For goals of the present study, a more
431 interesting finding is that the values of S_{max} calculated using NA are substantially larger than S_w
432 calculated at model level associated to the cloud base in ST. The difference between NA and ST in
433 the supersaturation values leads to a substantial difference in the droplet concentrations, especially
434 in cases of high CCN concentration. Calculation of S_{max} at cloud base changes the vertical profile
435 of supersaturation above it. While in ST supersaturation changes only slightly or even increase
436 with height within 100-200 m above cloud base, in NA supersaturation decreases within this layer
437 above the supersaturation maximum in agreement with the theory (Rogers and Yau, 1989, Pinsky
438 et al, 2012, 2013).

439 To justify the values of supersaturation and droplet concentration obtained in NA,
440 benchmark simulations using a parcel model were performed. The parcel model describes AP and
441 drops using drop size distribution defined on a mass grid containing 2000 mass bins (Pinsky et al,
442 2002). It calculates growth of AP and droplets by solving the equation for diffusional growth
443 written in the most general form without using parameterization of droplet nucleation. Time step
444 used for solving the diffusional growth equation was 0.001 s. The model was used earlier for
445 developing lookup tables relating parameters of AP and vertical velocity to droplet concentration
446 (Segal and Khain, 2006). Simulations with the parcel model were performed for the same vertical
447 velocity at cloud base, temperature and CCN distributions as in the HUCM simulations. As can be
448 seen from Fig. 2, the values of supersaturation and droplet concentration calculated using NA are
449 much closer to those calculated using the parcel model as compared to the values calculated using
450 ST.

451 The model level associated with the cloud base (where $S_w \geq 0$) is slightly higher than the
452 lifting condensation level (LCL), where $S_w = 0$. At the same time, the calculations performed
453 according to Pinsky et al. (2012) show that the level where $S_w = S_{\max}$ is located from about 20 m
454 (for high CCN concentration) to about 60 m (for low CCM concentration) higher than the LCL.
455 The estimations show, therefore, that the level where $S_w = S_{\max}$ is quite close to the model cloud
456 base level. Accordingly, the droplet concentration determined at $S_w = S_{\max}$ is assigned to the
457 corresponding grid point at the model cloud base.

458

459 **4.2 High CCN concentration**

460 In this section we compare the results for three pairs of simulations of clouds were
461 developing in a highly polluted atmosphere. **Figure 3** shows the fields of droplet concentration N_d
462 at the developing stage of the cloud evolution in E3500-S-0.5 (a), EN3500-S-0.5 (b), E3500-S (c)
463 and EN3500-S (d). The maximum N_d in NA is reached at cloud base, which makes the cloud base
464 well pronounced. The difference between droplet concentrations in ST and NA experiments
465 decreases with height. The highest droplet concentration is reached in simulations where the CCN
466 activation spectrum was characterized by the slope parameter $k=0.5$. This can be attributed to the
467 fact that at $k=0.5$ the aerosol spectrum contains more CCN which are activated at cloud base than
468 at $k=0.9$.

469 Vertical profiles of the maximum values of droplet concentration and of cloud water content
470 (CWC) averaged over time periods of storm development (a-b) and over the mature stage (c,d) are
471 presented in **Figure 4**.

472 In NA the N_d maximum is reached near cloud base and the droplet concentration decreases
473 with height.. This behavior of $N_d(z)$ is more realistic than in ST, where N_d increases with height
474 up to an altitudes 2- 4 km, depending on the stage of storm evolution. This increase in the N_d in
475 ST is caused by in-cloud activation of mid-size CCN which were not activated at cloud base in the
476 standard approach. In NA, these CCN were activated at cloud base. There is, therefore, a negative
477 feedback in the supersaturation-droplet concentration relationship: an underestimation of
478 supersaturation at low levels in the ST simulations leads to the underestimation of droplet
479 concentration and to the corresponding increase in supersaturation at comparatively small
480 distances above cloud base. These results indicate that in models where droplet nucleation is
481 calculated only at cloud base, the correct calculation of S_{\max} at cloud base is *strictly necessary to*
482 *obtain reasonable values of N_d in clouds.*

483 At height of about 4-5 kms, droplet concentrations in ST and NA become nearly similar.
484 Figs. 4a,c show also that N_d is very sensitive to the slope parameter of the CCN activation
485 spectrum. The maximum N_d reached at cloud base is about 1100 cm^{-3} in EN3500-S-05 ($k=0.5$)
486 as compared to $\sim 550\text{ cm}^{-3}$ in EN3500-S ($k=0.9$). This difference is caused by the fact that in case
487 $k=0.5$ the concentration of CCN with sizes exceeding $\sim 0.015\ \mu\text{m}$ (which are activated at cloud
488 base) is larger than in case $k=0.9$ (see Fig.1).

489 The effect of the *smallest* CCN on N_d (and on entire ice microphysical structure) becomes
490 very important above 6 km. In simulations containing the smallest CCN, these CCN are activated
491 producing new small droplets at heights of around 6.5- 8 km. The increase in N_d is shown in Fig.
492 4a,c by red arrows. These smallest CCN are not activated at cloud base even in NA (where S_{\max}
493 is larger than S_w in ST). This in-cloud nucleation is caused by an increase in supersaturation at

494 these levels due to a decrease in CWC (Fig. 4b,d) and an increase in vertical velocity (not shown).
495 The increase in N_d by activation at high levels and its effect on concentration of ice crystals in
496 cloud anvils of deep convective clouds was also reported by Khain et al. (2012).

497 Since the slope parameter determines concentration both of larger CCN and of smallest
498 CCN, the slope parameter also affects the concentration of droplets nucleated at high levels.

499 Vertical profiles of CWC (Figs. 4b,d) are typical of deep convective clouds developing in
500 the highly polluted environment: CWC is large and has maximum at about 5 km, i.e. at quite high
501 altitude.

502 **Figure 5a** shows the vertical profiles of maximum concentration of plate crystals (in HUCM
503 homogeneous freezing leads to formation of plates) averaged over the mature stage of cloud
504 evolution (from 4860 to 5460s). The number concentration of ice crystals in E3500 and EN3500
505 (in which there are no the smallest CCN in the initial CCN spectrum) is by factor of 5 lower than
506 in simulations with the CCN spectra containing the smallest CCN. The results show that ice
507 crystal concentration in NA is higher only slightly than in ST. Thus *the concentration of ice*
508 *crystals in cloud anvils is determined to a large extent by the concentration of smallest CCN in*
509 *the CCN spectra and is substantially less sensitive to larger CCN, which are activated at cloud*
510 *base*. Figure 5b shows that this conclusion is valid for the entire period of the simulation. In
511 agreement with Fig. 4c, the concentration of plates increased when NA was used (**Fig. 5b**). The
512 comparative contribution of the smallest CCN and CCN additionally activated at the cloud base in
513 NA (as compared to ST) are shown in Fig. 5b by arrows.

514 **Figure 6** shows the vertical profiles of time averaged maximum mass contents of ice
515 crystals, snow, graupel and hail+freezing drops at the storm mature stage. The maximum

516 difference between ice crystal mass contents takes place at ~10-11 km, where ice crystals are
517 caused by homogeneous freezing.

518 The most pronounced effect of NA is an increase in the accretion rate. In agreement with
519 results of simulations of aerosol effects on ice microstructure of deep convective clouds (Khain
520 2009; Tao et al. 2012; Khain et al. 2016), the intensification of riming leads to a decrease in the
521 snow mass content and to an increase in the mass contents of graupel (Fig.6b-c).. The existence of
522 the smallest CCN concentration leads to further decrease in the snow mass content and to the
523 increase in the graupel mass content. This smallest CCN lead to higher supercooled droplet
524 concentration and to an increase in the liquid mass available for riming (Fig. 4d,e).

525

526 **4.3. Low CCN concentration**

527 In this section we compare the results for three pairs of simulations: a) E100 and EN100, b)
528 E100-S and EN100-S, and c) E100-S-0.5 and EN100-S-0.5 in which clouds were developed in the
529 atmosphere with low CCN concentration. After the first 35 min of cloud evolution, the cloud base
530 is located at 700-800 m altitude and $T=16.8^{\circ}\text{C}$ at this level.

531

532 The fields of droplet concentration N_d in different simulations at the developing stage of the
533 cloud evolution are shown in **Figure 7**. The maximum N_d in a NA is reached at cloud base, which
534 makes the cloud base well pronounced. The difference in droplet concentrations between ST and
535 NA simulations decreases with height. Although the difference is N_d between NA and ST is very
536 pronounced, the absolute difference is not large (about 20 cm^{-3}). This low N_d determines a
537 typical maritime microphysical structure of clouds in both NA and ST cases.

538 **Figure 8** shows vertical profiles of the maximum values of droplet concentration and cloud
539 water content (CWC) averaged over the time period of 3420-4020s (mature stage). One can see a
540 dramatic difference in the profiles of droplet concentration and between CWC values of at low
541 CCN concentration as compared to high CCN concentration (Fig. 4). At low CCN concentration,
542 droplet collisions are efficient and droplet concentration decreases with height much faster than in
543 polluted air. As a result, the CWC maximum at low CCN concentration is located at the height of
544 2 km as compared to 5 km in case of high CCN concentration. These differences determine the
545 huge difference in the ice microphysics.

546 Fig. 8 shows that both the droplet concentration and CWC are larger in NA as compared to
547 ST. The main differences between droplet concentrations near cloud base are, however,
548 determined by the difference in the slope parameter value: at $k=0.5$ there are more CCN of sizes
549 exceeding $0.015 \mu m$ than at $k=0.9$ (Fig. 1). These CCN are activated at cloud base leading to
550 higher concentration in simulations with $k=0.5$, especially when NA was applied.

551 Efficient collisions (seen by the sharp decrease in the CWC above $z=2$ km) and rain fall
552 decrease the droplet concentration. As a result, the supersaturation increases and leads to in-cloud
553 nucleation and an increase in the droplet concentration already at distances of a few hundred
554 meters above the cloud base. However, since the concentration of CCN is low, the amount of
555 new nucleated droplets in the simulations was only about $5-10 \text{ cm}^{-3}$. The second layer of intense
556 in-cloud nucleation caused by activation of the smallest CCN is seen within the altitude layer from
557 4 km to 8 km. The difference in droplet concentration within this layer is fully related to the
558 existence/absence of smallest CCN in the CCN size spectrum. The differences between droplet
559 concentration in ST and NA simulations are not significant at these levels.

560 This result agrees with the case of high CCN concentration when droplet concentration at
561 higher levels is to a large extent determined by the smallest CCN in the droplet spectrum.

562 **Figure 9** presents the vertical profiles of maximum mass contents of ice crystals, snow,
563 graupel and hail + freezing drops at the mature stage of cloud evolution. Comparison with Fig. 6
564 shows that with the exception of snow, the mass contents of different ice hydrometeors at low
565 CCN concentration are substantially lower than at high CCN concentration. The main reason for
566 such difference is lower CWC at low CCN concentration that leads to less intense riming and,
567 consequently to slow growth of ice particles.

568 Fig. 9 shows that the profiles of ice hydrometeors in NA and ST are similar. It means that
569 the ice microphysics is to a large extent determined by the mass of supercooled droplets at high
570 levels which in turn is determined by the *smallest* CCN in the CCN size spectrum. The effects of
571 the smallest CCN and the shape of CCN size spectra on droplet concentration and the
572 concentration on ice microphysics are much stronger than the effect of additional droplets
573 nucleating at cloud base in the NA. The reason for this effect was explained above.

574 The increase in the concentration of the smallest CCN and in droplet concentration leads to
575 an increase in the ice crystals mass content occurring about the level of homogeneous freezing
576 (Fig.9a).

577 The mass content of snow decreases with the increase in the smallest CCN concentration ,
578 because intensification of riming of snow leads to its conversion to graupel (Fig. 9b).
579 Consequently, the graupel mass content increases (Fig. 9c). As regards to mass content of hail,
580 the increase in the smallest CCN concentration leads to a decrease in the hail content above 6 km
581 and to its increase below this level (Fig. 9d). The higher hail mass content above 6 km layer in
582 the absence of smallest CCN is likely related to the fact the low droplet concentration leads to

583 formation of raindrops in high concentration. Although these raindrops are of comparatively small
584 size, the total raindrop mass content is larger than that in case of higher drop concentration. These
585 raindrops rapidly freeze above the freezing level producing hail (actually frozen drops) with total
586 mass larger than at high CCN concentration. This effect is discussed by Iltovich et al. (2016) in
587 detail. In HUCM, frozen raindrops are assigned to the hail category due to their high density. If
588 hail is defined as particles with sizes exceeding 1 cm, the amount of hail at low CCN
589 concentration would be negligible.

590

591 Higher hail mass content below 6 km in the presence of the smallest CCN can be attributed
592 to intense conversion of heavy rimed graupel to hail, as well as to more efficient hail growth by
593 riming. Note that sizes of hail particles forming in a deep convective cloud developing in the
594 polluted atmosphere are larger than hail forming in a cloud developing in clean air (Iltovich et al.
595 2016). Due to larger size, hail in the polluted case falls to the surface (Fig. 6d), while in clean air
596 hail melts at 1.5 km in the absence of small CCN, and in vicinity of the surface if the CCN size
597 spectrum contains the smallest CCN.

598 4.3 The impact on precipitation

599 **Figure 10a** shows the accumulated rain at surface in the polluted air. Accumulated rain
600 is maximum in EN3500-S-0.5 where effect of smallest CCNs is combined with the effect of
601 comparatively large amount of large CCN. This synergetic effect of the smallest and large CCN
602 is described by Khain et al. (2011). In most simulations, the masses of accumulated rain are
603 quite similar.

604 Comparison of Fig. 10a and Fig. 10 b shows that the accumulated rain at low aerosol
605 concentration is lower than at high CCN concentration, which is in agreement with many

606 previous studies. Accumulated rain in NA was found to be quite close to that in ST. The main
607 difference in the values of accumulated rain at low CCN concentration is caused by effects of
608 smallest aerosols increasing the mass of precipitating ice particles .

609 Amount of hail at the surface in polluted air (**Figure 10c**) is substantially larger than in
610 clean air (**Figure 10d**) due to lower sizes and faster melting of hail particles if CCN
611 concentration is low. The effect of AP on the size and amount of hail at the surface was
612 investigated by Ilotovich et al. (2016) in detail.

613 Amount of hail at the surface in polluted air is slightly higher in EN3500-S-0.5 as
614 compared to E3500-S-0.5 (**Figure 10c**). We attribute this effect to a higher rate of riming in
615 EN3500-S-0.5 due to a higher amount of supercooled water (Fig. 4b, d). There are no
616 significant differences in the other cases of polluted air.

617 The main factor determining the differences in the amount of hail falling to the surface at
618 low CCN concentration is the effect of smallest CCN. The increase in concentration of smallest
619 CCN leads to an increase in hail growth by riming.

620 As regards to the ratio of hail amounts in the experiments with smallest AP, earlier or later
621 intensification of convective cells (which is more or less random) may affect the ratio. Since
622 the mass of hail falling to the surface in clean air is very low, a larger computational area is
623 required to obtain reliable statistics.

624

625 5. Conclusions

626 Sensitivity of the microphysics of deep convective clouds to the concentration of aerosols and
627 to the shape of aerosol size distribution is investigated using a new version of a 2D Spectral (bin)
628 Microphysics Cloud Model (HUCM). A new component of the model is the calculation of

629 maximum supersaturation at cloud base using the analytical expression derived by Pinsky et al.
630 (2012). The cloud microphysical structure obtained using this expression is compared with that
631 obtained with supersaturation calculated at model grid points.

632 The goal of the study was twofold: a) to test the effects of the improved calculation of
633 supersaturation maximum near cloud base (NA (new approach) vs ST (standard approach)) at
634 different aerosol loadings and b) to evaluate sensitivity of cloud microphysics to concentration and
635 shape of size distribution of aerosol particles. In the simulations, shape of CCN size distributions
636 was changed by changing the value of the slope parameter in the expression for activation
637 spectrum (the values of $k=0.5$ and $k=0.8$ were used) and by adding the smallest CCN with radii
638 below $0.015 \mu m$.

639 The values of S_{max} near cloud base calculated by the theoretical analysis were found to be
640 substantially larger than the supersaturation values calculated explicitly at model grid points
641 associated with cloud base. The comparison of the values of supersaturation at cloud base and
642 droplet concentration in the model simulations with the corresponding values calculated using a
643 benchmark parcel model showed that NA simulates cloud base supersaturation and droplet
644 concentration much more accurately than ST. Thus, *the first main conclusion* of the study is that
645 the droplet concentration field in NA is substantially more realistic than in ST, with the maximum
646 of droplet concentration in NA located near cloud base in agreement with classical results (Rogers
647 and Yau, 1989). The increased droplet concentration makes the cloud base more pronounced. The
648 improvement of the representation of the vertical profile of the droplet concentration is especially
649 significant in case of high CCN concentration, where utilization of S_{max} leads to a substantial
650 increase in the concentration of droplets near cloud base. Thus, even at 100-m vertical resolution,

651 it is necessary to use analytical expressions for S_{\max} . At low CCN concentration, the improved
652 representation of droplet concentration above cloud base has a comparatively weak effect on cloud
653 microphysics. This result can be attributed to the fact that droplet concentration increases
654 relatively slightly if it is more accurately calculated since the available CCN concentration is low.
655 As a result, intense warm rain rapidly arises in both NA and ST.

656 The error in calculation of droplet concentration near cloud base in ST is compensated to a
657 significant extent by in-cloud nucleation above cloud base. Indeed, in NA droplet concentration
658 increases with height up to level of 4 km (Fig. 4a). The only reason of such increase is the in-cloud
659 nucleation of comparatively large CCN.

660 Models with microphysical schemes that do not describe in-cloud droplet nucleation should
661 include calculation of S_{\max} at cloud base to avoid large errors in simulation of the microphysical
662 cloud structure.

663 *The second main conclusion* is high importance of the shape of CCN size distribution. Cloud
664 microphysics was found to be highly sensitive to the slope parameter of the CCN activation
665 spectra. The effect is comparable with the change in the total CCN concentration via the change
666 in the intercept parameter N_0 . The utilization of $k=0.5$ instead of $k=0.9$ nearly doubled droplet
667 concentration near cloud base that leads to corresponding effects on cloud microphysics, in
668 particular, to an increase in accumulated rain.

669 *The third main conclusion* is high sensitivity of ice microphysics to the existence of the
670 smallest CCN in the CCN size spectrum. Both in cases of low and high CCN concentration, the
671 differences in ice microphysics are determined to a large extent by *concentration of the smallest*
672 *aerosols in the CCN spectra*. In cases of high CCN concentration, the effect of the smallest CCN

673 in the NA becomes important above 5-6 km altitude where they are activated producing additional
674 supercooled liquid droplets. The latter leads to the increase in the concentration of ice crystals
675 above the level of homogeneous freezing by factor of about 5, to doubling of graupel mass
676 maximum. The smallest CCN also influence hail size and mass content.

677 In case of low CCN concentration the smallest CCN also lead to an increase in the
678 concentration and mass contents of ice crystals and to a significant increase of graupel and hail
679 mass contents. Note that many probes of CCN measure concentration of CCN at supersaturations
680 not exceeding 0.6%. In this case the concentration of the smallest CCN which remain non-
681 activated at this supersaturation remains unknown. Such measurements do not provide necessary
682 information for investigation of mixed-phase and ice microphysics.

683 Accumulated rain amount in case of high CCN concentration turned out to be higher than in
684 case of low CCN concentration. This result was discussed by Khain (2009) and Iltovich et
685 al.(2016) showing that formation of hail increases precipitation efficiency of mid-latitude storms.

686 Ice precipitation (calculated in mm of melted hail) at the surface is much lower than liquid
687 precipitation. Nevertheless, hail precipitation at the surface in case of high CCN concentration is
688 higher than in case of low CCN concentration by order of magnitude in agreement with results by
689 Khain et al. (2011) and Iltoviz et al. (2016). This effect can be attributed by formation of larger
690 hail particles in case of high CCN concentration (high supercooled mass content). The large hail
691 particles reach the surface, while smaller hail forming in case of low CCN concentration melts
692 without reaching the surface.

693 The concentrations of drops and ice crystals are important parameters determining cloud
694 radiative properties. In this context, more accurate calculation of the concentrations using the NA

695 as well as taking into account the effects of smallest CCN should improve the accuracy of
696 evaluation of radiative cloud properties. The proposed approach of calculation of nucleation of
697 droplets at cloud base is simple in the utilization and computationally efficient. It can be used in
698 cloud-resolved models with different vertical grid spacing. The utilization of cruder vertical model
699 resolution may lead to larger errors in cases when droplet concentration at cloud base is calculated
700 using supersaturations calculated at model grid points.

701 *Acknowledgements*

702 The study is supported by the US Department of Energy Award DE_FOA-0000647 from the U.S.
703 Department of Energy Atmospheric System Research Program, by the Binational US-Israel
704 Science Foundation (grant 2010446), and by the Israel Science Foundation (grant 1393/14).

705

706 **Appendix. Derivation of an expression for the supersaturation maximum at cloud base**

707 Detailed description of the derivation of Eq. (1) is given in Pinsky et al. (2012). Below we present
708 only a short description. Assuming that near cloud base $S_w \ll 1$, the equation for supersaturation
709 can be written as:

710

$$711 \quad \frac{dS_w}{dt} = A_1 \frac{dz}{dt} - A_2 \frac{dq_w}{dt} \quad (A1)$$

712

713 where coefficients A_1 and A_2 are presented in **Table 1**; z is the height above cloud base and q_w
714 is liquid water mixing ratio. The first term on the right-hand side of eq. (A1) describes an
715 increase in supersaturation due to adiabatic air cooling during ascent, whereas the second term

716 describes the supersaturation decrease caused by condensation of water vapor on droplets.

717 Integration of equation (A1) leads to the equation of mass balance:

$$718 \quad S_w = A_1 z - A_2 q_w + C_1 \quad (A2)$$

719 where $C_1 = 0$ at cloud base. Assuming monodisperse DSD with droplets of radii r , the liquid

720 water mixing ratio can be written as :

$$721 \quad q_w = \frac{4}{3} \pi \frac{\rho_w}{\rho_a} N_d r^3 \quad (A3)$$

722 where N_d is the droplet concentration. The equation for diffusional growth can be written is the

723 form where the curvature term and the chemical term are omitted (Pinsky et al. 2012):

$$724 \quad \frac{dr}{dt} = \frac{1}{Fr} S_w \quad (A4)$$

725 The expression for coefficient F is presented in **Table 1**. Coefficients A_1 , A_2 and F slightly

726 depend on temperature and can be assumed constant in the analysis. Using Eqs. (A2-A4), eq. (1)

727 can be rewritten in the closed form as:

$$728 \quad \frac{dS_w}{dz} = A_1 - \frac{1}{w} B_1 (A_2 N_d)^{2/3} (A_1 z - S_w)^{1/3} S_w \quad (A5)$$

$$729 \quad \text{where } B_1 = \frac{3}{F} \left(\frac{4\pi \rho_w}{3 \rho_a} \right)^{2/3}$$

730 Pinsky et al. (2012) showed that Eq. (A5) can be written in a non-dimensional form that

731 results in an universal profile of supersaturation with height at given vertical velocity. The

732 condition $\frac{dS_w}{dz} = 0$ applied to this equation allows to get solution in the form (1) for S_{\max} , as

733 well as for the height of S_{\max} over the cloud base. Pinsky et al. (2012, 2014) showed that (1) is

734 valid for any size distributions of CCN.

735

736

737

738

739

740

741

742

743

744

745

746

747

748

749

750

751

752 **References**

753 Abdul-Razzak, H., and S. J. Ghan (2000), A parameterization of aerosol activation: 2.
754 Multiple aerosol types, *J. Geophys. Res.*, *105*(D5), 6837, doi:10.1029/1999JD901161.

755 Abdul-Razzak, H., S. J. Ghan, and C. Rivera-Carpio (1998), A parameterization of aerosol
756 activation: 1. Single aerosol type, *J. Geophys. Res.*, *103*(D6), 6123, doi:10.1029/97JD03735.

757 Benmoshe, N., M. Pinsky, A. Pokrovsky, and A. Khain, 2012: Turbulent effects on the
758 microphysics and initiation of warm rain in deep convective clouds: 2-D simulations by a
759 spectral mixed-phase microphysics cloud model. *J. Geophys. Res.*, **117**, D06220,
760 doi:10.1029/2011JD016603.

761 Bedos, C., K. Suhre, and R. Rosset (1996), Adaptation of a cloud activation scheme to a
762 spectral-chemical aerosol model, *Atmos. Res.*, *41*(3-4), 267–279, doi:10.1016/0169-
763 8095(96)00014-2.

764 Bigg, E. K., 1953: The formation of atmospheric ice crystals by the freezing of droplets.
765 *Quart. J. Roy. Meteor. Soc.*, *79*, 510–519, doi:10.1002/qj.49707934207.

766 Cohard, J.-M., J.-P. Pinty, and C. Bedos (1998), Extending Twomey's Analytical Estimate
767 of Nucleated Cloud Droplet Concentrations from CCN Spectra, *J. Atmos. Sci.*, *55*(22), 3348–
768 3357, doi:10.1175/1520-0469(1998)055<3348:ETSAEO>2.0.CO;2.

769 Fountoukis, C. (2005), Continued development of a cloud droplet formation
770 parameterization for global climate models, *J. Geophys. Res.*, *110*(D11), D11212,
771 doi:10.1029/2004JD005591.

772 Freud E., and D. Rosenfeld, 2012: Linear relation between convective cloud drop
773 number concentration and depth for rain initiation. *J. Geophys. Res.* **117**, D02207.

774 Ghan, S. J., C. C. Chung, and J. E. Penner (1993), A parameterization of cloud droplet
775 nucleation part I: single aerosol type, *Atmos. Res.*, *30*(4), 198–221, doi:10.1016/0169-
776 8095(93)90024-I.

777 Ghan, S. J., L. R. Leung, R. C. Easter, and H. Abdul-Razzak (1997), Prediction of cloud
778 droplet number in a general circulation model, *J. Geophys. Res.*, *102*(D18), 21777,
779 doi:10.1029/97JD01810.

780 Ghan, S. J., H. Abdul-Razzak, A. Nenes, Y. Ming, X. Liu, M. Ovchinnikov, B. Shipway,
781 N. Meskhidze, J. Xu, and X. Shi (2011), Droplet nucleation: Physically-based
782 parameterizations and comparative evaluation, *J. Adv. Model. Earth Syst.*, *3*(4), n/a–n/a,
783 doi:10.1029/2011MS000074.

784 Heymsfield A. J., A. Bansemer, G. Heymsfield and A.O. Fierro (2009), Microphysics of
785 maritime tropical convective updrafts at temperatures from -20 oC to -60 oC, *J. Atmos. Sci.*, *66*,
786 3530-3565.

787 Iltoviz, E., A. Khain, N. Benmoshe, V. T. J. Phillips, and A. Ryzhkov, 2016: Effect of
788 aerosols on freezing drops, hail and precipitation in a mid-latitude storm. *J. Atmos. Sci.*, *73*,
789 109-144, <http://dx.doi.org/10.1175/JAS-D-14-0155.1>.

790 Khain, A. P., 2009: Notes on state-of-the-art investigations of aerosol effects on
791 precipitation: A critical review. *Environ.Res. Lett.*, 4, 015004, doi:10.1088/1748-
792 9326/4/1/015004.

793 Khain, A., M. Ovtchinnikov, M. Pinsky, A. Pokrovsky, and H. Krugliak (2000), Notes on
794 the state-of-the-art numerical modeling of cloud microphysics, *Atmos. Res.*, **55**(3-4), 159–224,
795 doi:10.1016/S0169-8095(00)00064-8.

796 Khain, A. P., Benmoshe, N. and A. Pokrovsky, 2008: Factors Determining the Impact of
797 Aerosols on Surface Precipitation from Clouds: An Attempt at Classification, *J. Atmos. Sci.*,
798 65(6), 1721–1748, doi:10.1175/2007JAS2515.1.

799 Khain, A.P., D. Rosenfeld, A. Pokrovsky, U. Blahak, and A. Ryzhkov (2011), The role of
800 CCN in precipitation and hail in a mid-latitude storm as seen in simulations using a spectral
801 (bin) microphysics model in a 2D dynamic frame, *Atmos. Res.*, 99(1), 129–146,
802 doi:10.1016/j.atmosres.2010.09.015.

803 Khain, A.P., V. Phillips, N. Benmoshe, and a. Pokrovsky, 2012: The Role of Small Soluble
804 Aerosols in the Microphysics of Deep Clean Clouds, *J. Atmos. Sci.*, 69(9), 2787–2807,
805 doi:10.1175/2011JAS3649.1.

806 Khain A.and B. Lynn And J. Shpund, 2016: High Resolution WRF Simulations of
807 Hurricane Irene: Sensitivity to Aerosols and Choice of Microphysical schemes. *Atmos.*
808 *Research*. Volume 167, 1 January 2016, 129–145.

809 Khvorostyanov, V. I., and J. a. Curry (2006), Aerosol size spectra and CCN activity
810 spectra: Reconciling the lognormal, algebraic, and power laws, *J. Geophys. Res.*, *111*(D12),
811 D12202, doi:10.1029/2005JD006532.

812 Kogan Y.L. 1991: The simulation of a convective cloud in a 3-D model with explicit
813 microphysics. Part I: Model description and sensitivity experiments. *J. Atmos. Sci.*, **48**,
814 1160–1189.

815 Meyers, M. P., P. J. DeMott, and W. R. Cotton, 1992: New primary ice-nucleation
816 parameterizations in an explicit cloud model. *J. Appl. Meteor.*, **31**, 708–721.

817 Phillips, V. T. J., A. Pokrovsky, and A. Khain, 2007: The influence of time-dependent
818 melting on the dynamics and precipitation production in maritime and continental storm clouds.
819 *J. Atmos. Sci.*, **64**, 338–359, doi:10.1175/JAS3832.1.

820 Phillips, V. T. J., A. Khain, N. Benmoshe, A. Ryzhkov, and E. Iltovich, 2014: Theory of
821 time dependent freezing. Part I: Description of scheme for wet growth of hail. *J. Atmos. Sci.*,
822 **71**, 4527–4557, doi:10.1175/JAS-D-13-0375.1.

823 Phillips, V. T. J., A. Khain, N. Benmoshe, A. Ryzhkov, and E. Iltovich, 2015: Theory of
824 time dependent freezing. Part II: Scheme for freezing raindrops and simulations by a cloud
825 model with spectral bin microphysics. *J. Atmos. Sci.*, **72**, 262–286, doi:10.1175/JAS-D-13-
826 0376.1.

827 Pinsky, M., Khain, A. P.: 2002 Effects of in-cloud nucleation and turbulence on droplet spectrum
828 formation in cumulus clouds. *Quart. J. Roy. Met. Soc.*, *128*, 1-33.

829 Pinsky M., I. Mazin, A. Korolev and A. Khain (2012), Analytical estimation of droplet
830 concentration at cloud base, *J. Geophys. Res.* **117**, D18211, 14 PP.

831 Pinsky M., I.P. Mazin, A. Korolev , and A. Khain, 2013:Supersaturation and diffusional
832 droplet growth in liquid clouds. *J. Atmos. Sci.* **70**, 2778-2793

833 Pinsky M., I. Mazin, A. Korolev and A. Khain (2014) Supersaturation and diffusional
834 droplet growth in liquid clouds: Polydisperse spectra . *J. Geophys Res.* 2014, **119**, 12872-
835 12887.

836 Pruppacher, H.R., Klett, J.D., 1997. *Microphysics of Clouds and Precipitation*. 2nd edn.
837 Oxford Press, 914 p.

838 Rogers R. R. and Yau M. K, 1989: *A Short Course in Cloud Physics*, Pergamon press.
839 293pp.

840 Rosenfeld, D., U. Lohmann, G. B. Raga, C. D. O'Dowd, M. Kulmala, S. Fuzzi, A.
841 Reissell, and M. O. Andreae (2008), Flood or drought: how do aerosols affect precipitation?,
842 *Science*, **321**(5894), 1309–13, doi:10.1126/science.1160606.

843 Rotunno, R., and J. Klemp (1985), On the Rotation and Propagation of Simulated
844 Supercell Thunderstorms, *J. Atmos. Sci.*, **42**(3), 271–292, doi:10.1175/1520-
845 0469(1985)042<0271:OTRAPO>2.0.CO;2.

846 Segal Y. and Khain, A. P., 2006: Dependence of droplet concentration on aerosol
847 conditions in different cloud types: application to droplet concentration parameterization of
848 aerosol conditions, *J. Geophys. Res.* Vol. **111**, D15204, doi:10.1029/2005JD006561

849 Shipway, B. J., and S. J. Abel (2010), Analytical estimation of cloud droplet nucleation
850 based on an underlying aerosol population, *Atmos. Res.*, 96(2-3), 344–355,
851 doi:10.1016/j.atmosres.2009.10.005.

852 Takahashi, T., Endoh, T., Wakahama, G., 1991. Vapor diffusional growth of free-falling snow
853 crystals between -3 and -23°C . *J. Meteorol. Soc. Jpn.* 69, 15–30.

854 Tao W.-K., Jen-Ping Chen, Zhanqing Li, Chien Wang, Chidong Zhang (2012), Impact of
855 Aerosols on Convective Clouds and Precipitation. *Reviews of Geophysics*. [50, Issue 2](#), June
856 2012 DOI: 10.1029/2011RG000369.

857 Vali, G., 1994: Freezing rate due to heterogeneous nucleation. *J. Atmos. Sci.*, 51, 1843–
858 1856, doi:10.1175/1520-0469(1994)051,1843:FRDTHN.2.0.CO;2.

859

860

861

862

863

864

865

866

867

868 **Table 1. List of symbols**

869

870

Symbol	Description	Units
A	$\frac{2\sigma_w}{\rho_w R_v T}$	m
A_1	$\frac{g}{R_a T} \left(\frac{L_w R_a}{c_p R_v T} - 1 \right)$	m^{-1}
A_2	$\frac{1}{q_v} + \frac{L_w^2}{c_p R_v T^2}$	-
B	$\frac{v_n \Phi_s \varepsilon_m M_w \rho_n}{M_n \rho_w}$	-
B_1	$\frac{3}{F} \left(\frac{4\pi\rho_w}{3\rho_a} \right)^{2/3}$	$\text{m}^2 \text{s}$
C_1	$1.058 (FA_1 / 3)^{3/4} \left(\frac{3\rho_a}{4\pi\rho_w A_2} \right)^{1/2}$	$\text{m}^{9/4} \text{s}^{-3/4}$
c_p	specific heat capacity of moist air at constant pressure	$\text{J kg}^{-1} \text{K}^{-1}$
D	coefficient of water vapor diffusion in the air	$\text{m}^2 \text{s}^{-1}$
e		
e_w	saturation vapor pressure above the flat surface of water	N m^{-2}
g	acceleration of gravity	m s^{-2}
F	$\left(\frac{\rho_w L_w^2}{k_a R_v T^2} + \frac{\rho_w R_v T}{e_w(T)D} \right)$	$\text{m}^{-2} \text{s}$
K	parameter of activity spectra	
k_a	coefficient of air heat conductivity	$\text{J m}^{-1} \text{s}^{-1} \text{K}^{-1}$
L_w	latent heat for liquid water	J kg^{-1}
M_n	molecular weight of aerosol salt	kg mol^{-1}
M_w	molecular weight of water	kg mol^{-1}
N_d	concentration of liquid droplets	m^{-3}

N_0	parameter of activation spectra	
P	pressure of moist air	N m^{-2}
q_v	water vapor mixing ratio (air)	kg kg^{-1}
q_w	liquid water mixing ratio	kg kg^{-1}
r_{\max}	drop radius at $z = z_{\max}$	m
		-
S_w	$S_w = e/e_w - 1$ supersaturation over water	-
S_{\max}	supersaturation maximum	-
T	absolute temperature	$^{\circ}\text{K}$
T_C	temperature at cloud base	$^{\circ}\text{C}$
w	vertical velocity	m s^{-1}
z	height over condensation level	m
z_{\max}	height of supersaturation maximum	m
		-
ε_m	soluble fraction	-
		-
ρ_a	density of air	kg m^{-3}
ρ_N	density of a dry aerosol particle	kg m^{-3}
ρ_w	density of liquid water	kg m^{-3}
σ_w	surface tension of water-air interface	Nm^{-1}
		-
ν_n	van 't Hoff factor	-

871

872

873

874

875

876

877

878 **Table 2.** CCN concentrations in different experiments in the boundary layer

Slope parameter	High CCN concentration, cm^{-3}		Low CCN concentration, cm^{-3}	
	No smallest CCN	With smallest CCN	No smallest CCN	With smallest CCN
k=0.9	840	2930	33	214
k=0.5	1552	3140	53	152

879

880

881

882

883

884

885

886

887

888

889

890

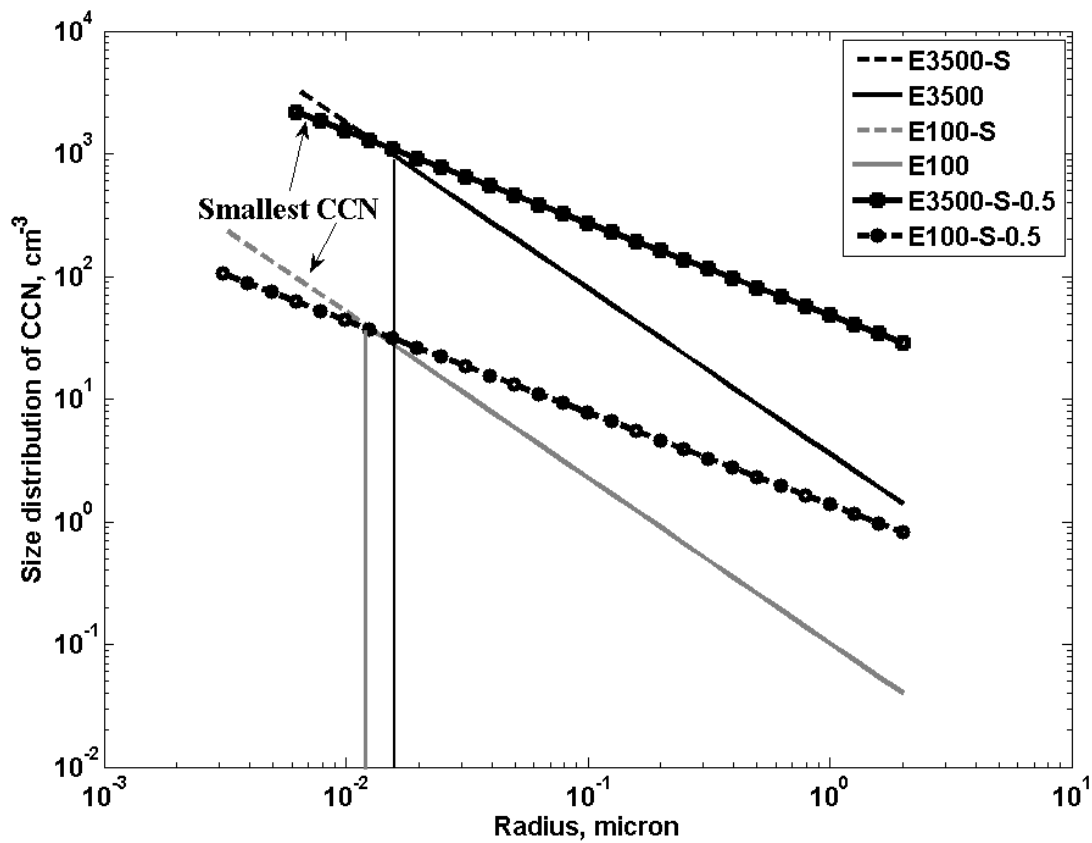
891

892

893

894 **Figures**

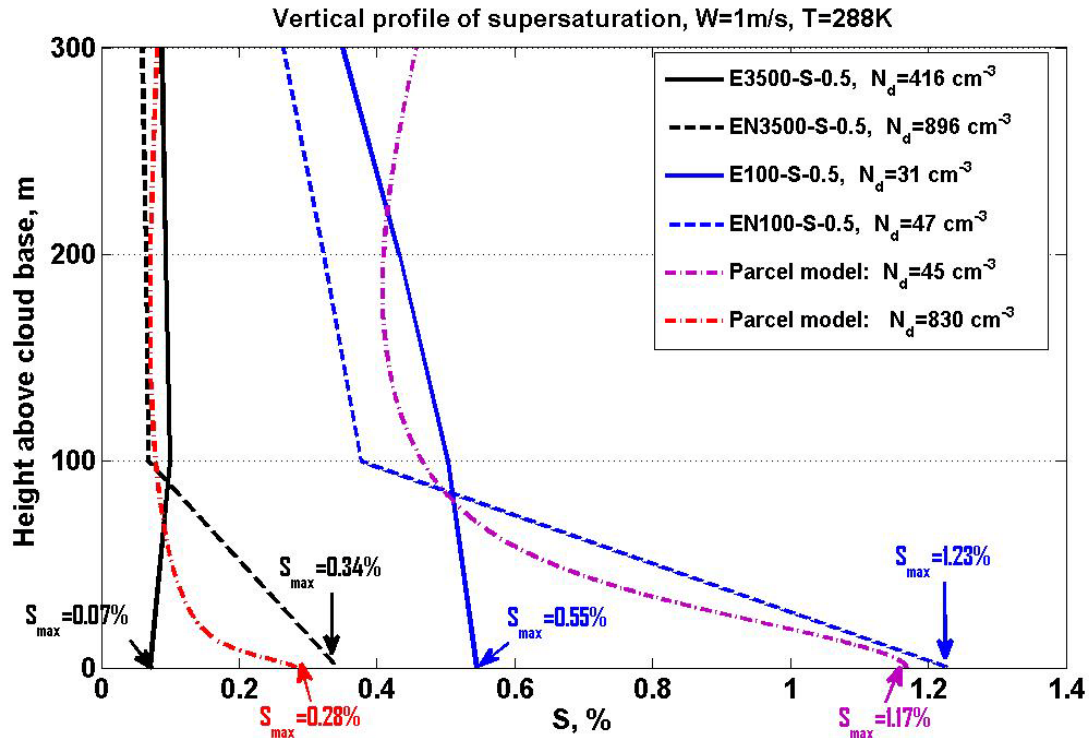
895



896

897 **Figure 1.** The initial size distributions of aerosols near the surface in different simulations.

898



899

900 **Figure 2.** Examples of vertical profiles of the supersaturation above cloud base calculated using
 901 HUCM and a benchmark parcel model. The columns with w close to 1 m/s at cloud base were
 902 chosen for comparison. The values of S_{max} in HUCM were calculated according to *Pinsky et al.*
 903 (2012). The values of droplets concentration calculated at cloud base in different simulations
 904 are shown as well (see legend box).

905

906

907

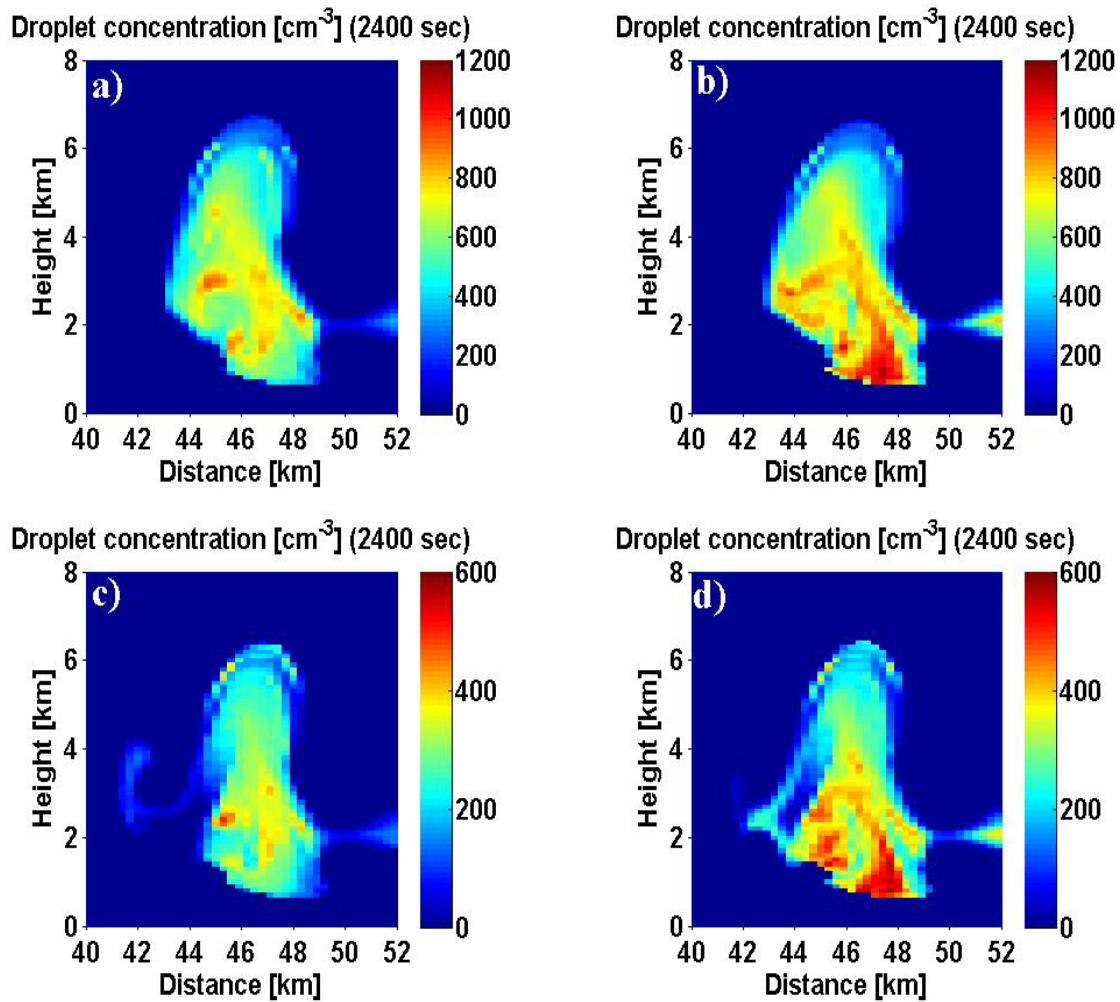
908

909

910

911

912



914

915

916

917 **Figure 3.** Field of droplet concentration at $t=2400$ s in (a) E3500-S-0.5, (b) EN3500-S-0.5, (c)

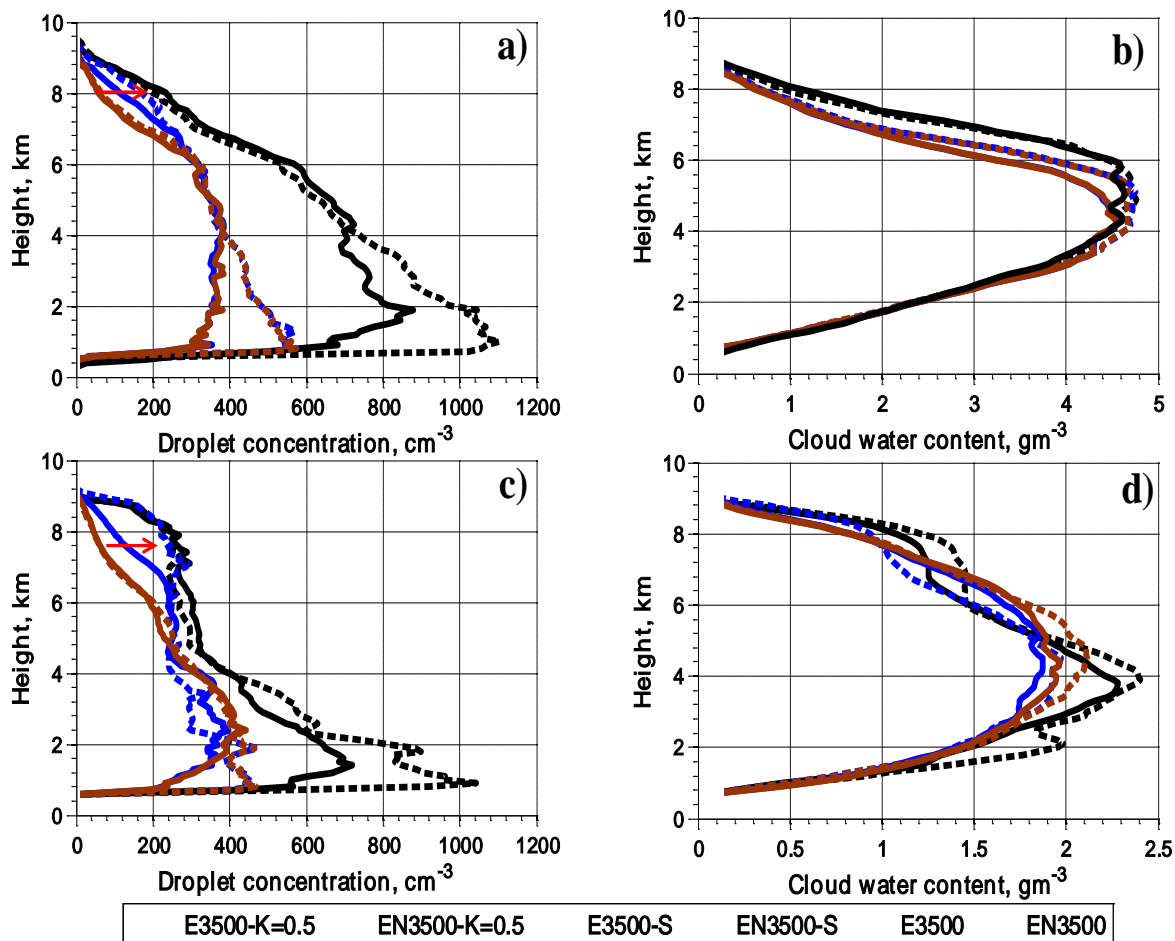
918 E3500-S and (d) EN3500-S.

919

920

921

922



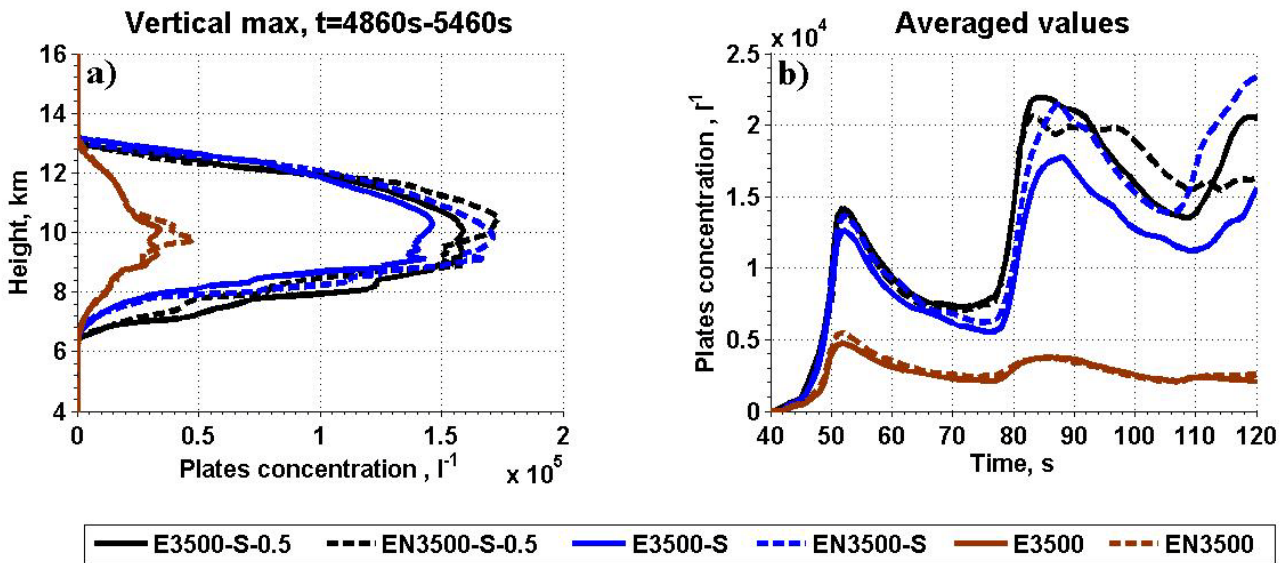
924

925

926 **Figure 4.** Vertical profiles of the maximum values of droplet concentration (a,d) and CWC(b,e)
 927 in simulations with high CCN concentration. The profiles are obtained by averaging over the
 928 time period of 2400-3000s (upper row) and over time period of 4860-5460s (bottom row). Panel
 929 (c) shows a zoom of panel (b) for large CWC .

930

931



932

933

934

935

936 **Figure 5.** Vertical profiles of (a) maximum values of plates concentration and (b) time
 937 dependencies of averaged plate concentration. The profiles are obtained by averaging over the
 938 time period of 4860-5460s. The low and the upper arrows in the panel b show approximate
 939 contribution of smallest CCN and the additional CCN activated in NA, respectively.

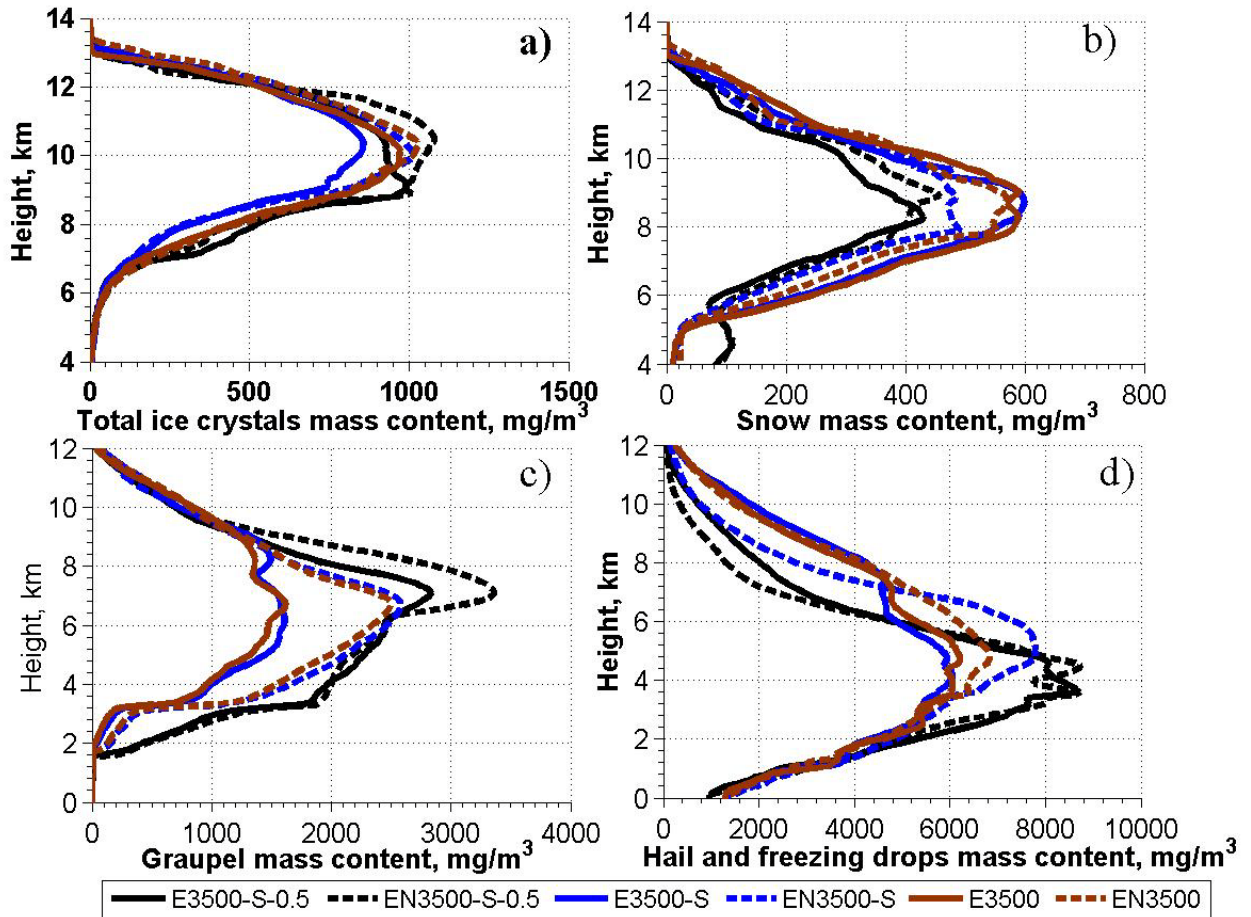
940

941

942

943

944



945

946

947 **Figure 6.** Vertical profiles of the maximum values of mass content: (a) total ice crystals, (b)
 948 snow, (c) graupel and (d) total hail and freezing drops in simulations with high CCN
 949 concentration. The profiles are obtained by averaging over the time period of 4860-5460s.

950

951

952

953

954

955

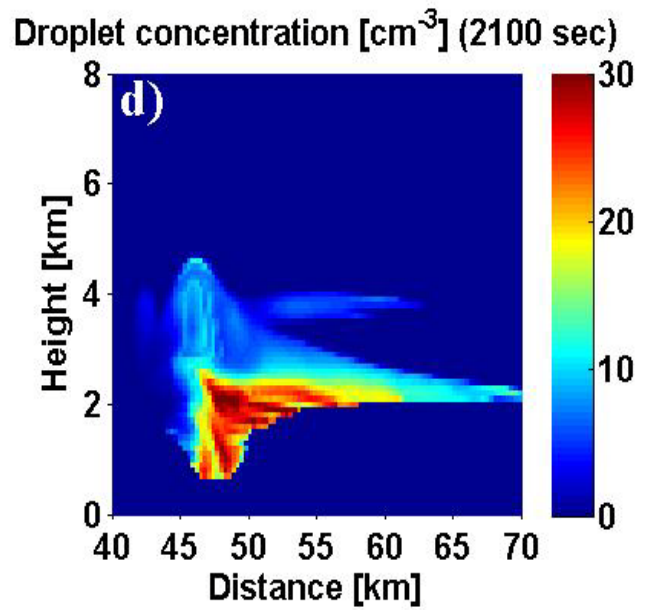
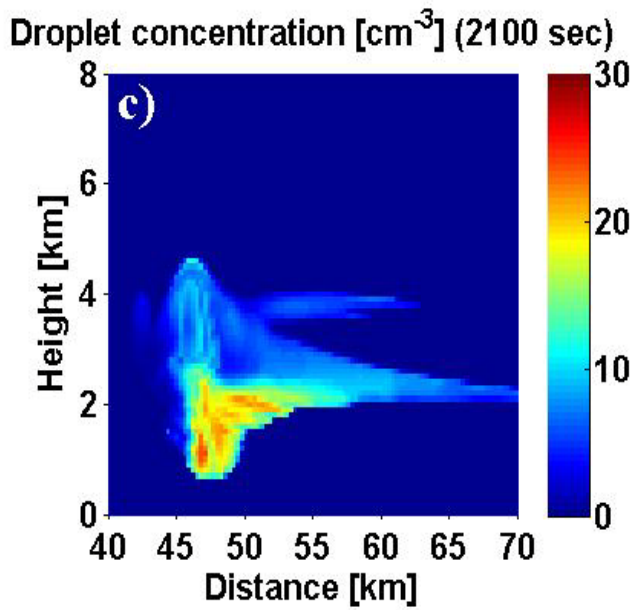
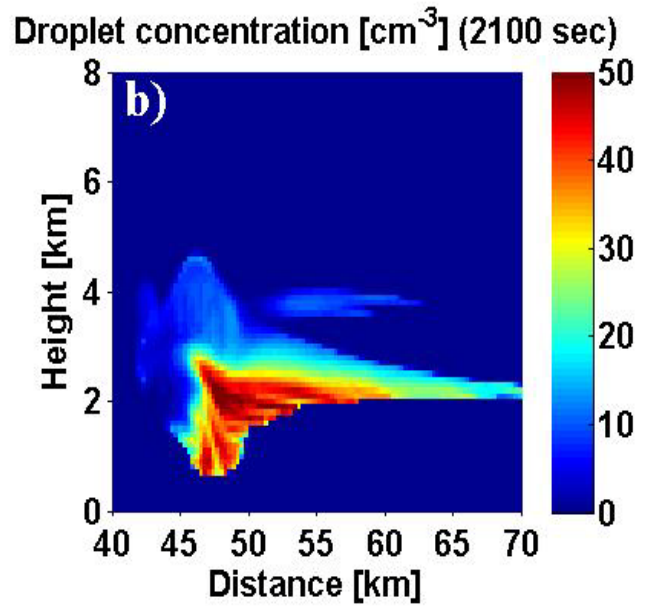
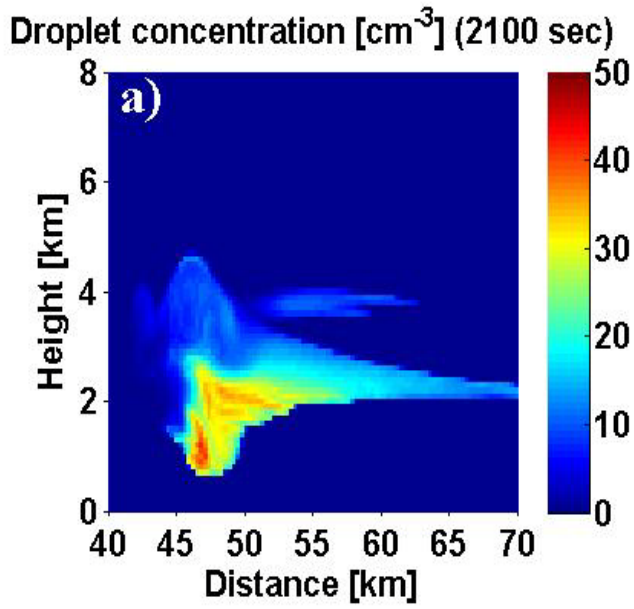
956

957

958

959

960



961

962

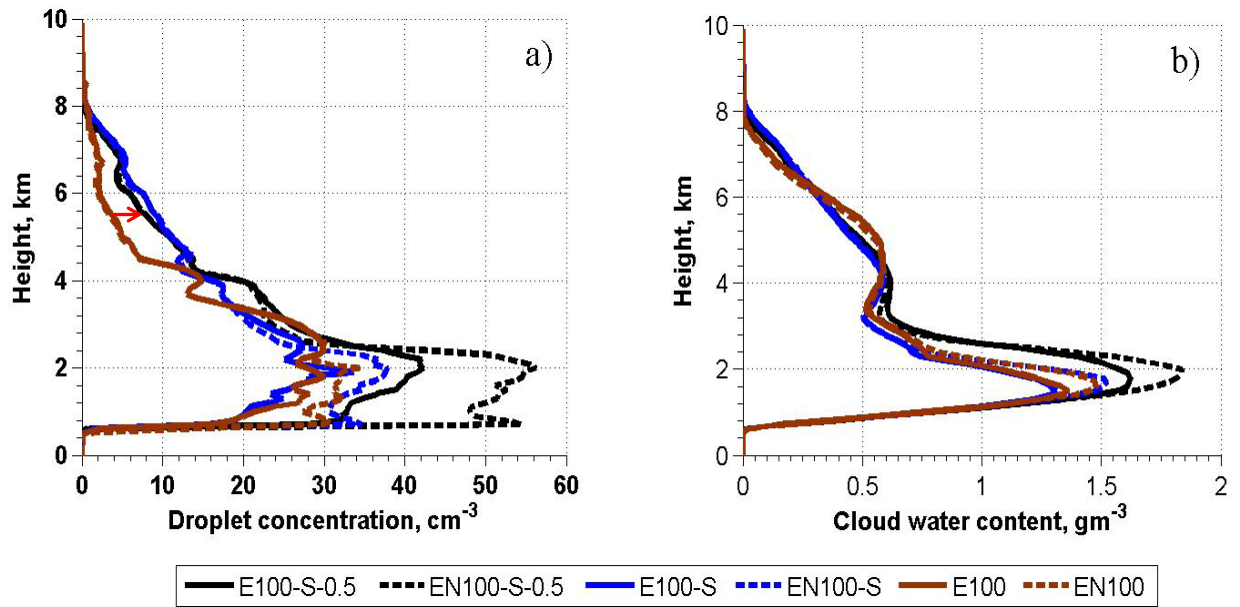
963

964 **Figure 7.** Field of droplet concentration at $t=2100\text{s}$ in (a) E100-S-0.5, (b) EN100-S-0.5, (c)
 965 E100-S and (d) EN100-S simulations.

966

967

968
969
970



971

972

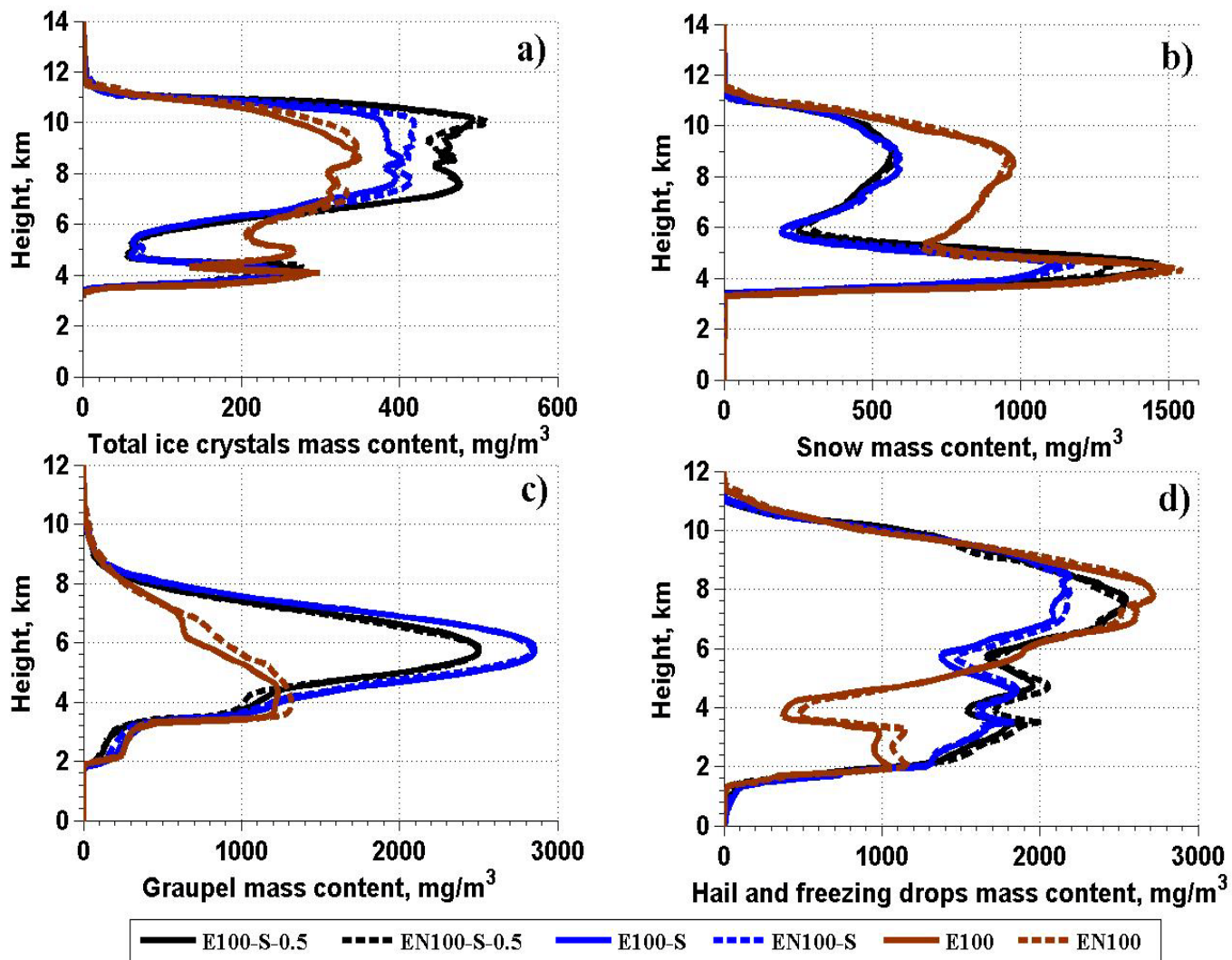
973 **Figure 8.** Vertical profiles of the maximum values of droplet concentration (a) and CWC (b) in
974 simulations with low CCN concentration ($N_0 = 100 \text{ cm}^{-3}$). The profiles are obtained by
975 averaging over the time period of 3420-4020s. Red arrow shows the increase in droplet
976 concentration due to in-cloud nucleation in simulations with the CCN spectra containing small
977 CCN.

978

979

980

981



982

983

984 **Figure 9.** Vertical profiles of the maximum values of mass content: (a) total ice crystals, (b)
 985 snow, (c) graupel and (d) total hail and freezing drops in the simulations with low CCN
 986 concentration. The profiles are obtained by averaging over the time period of 3420-4020s.

987

988

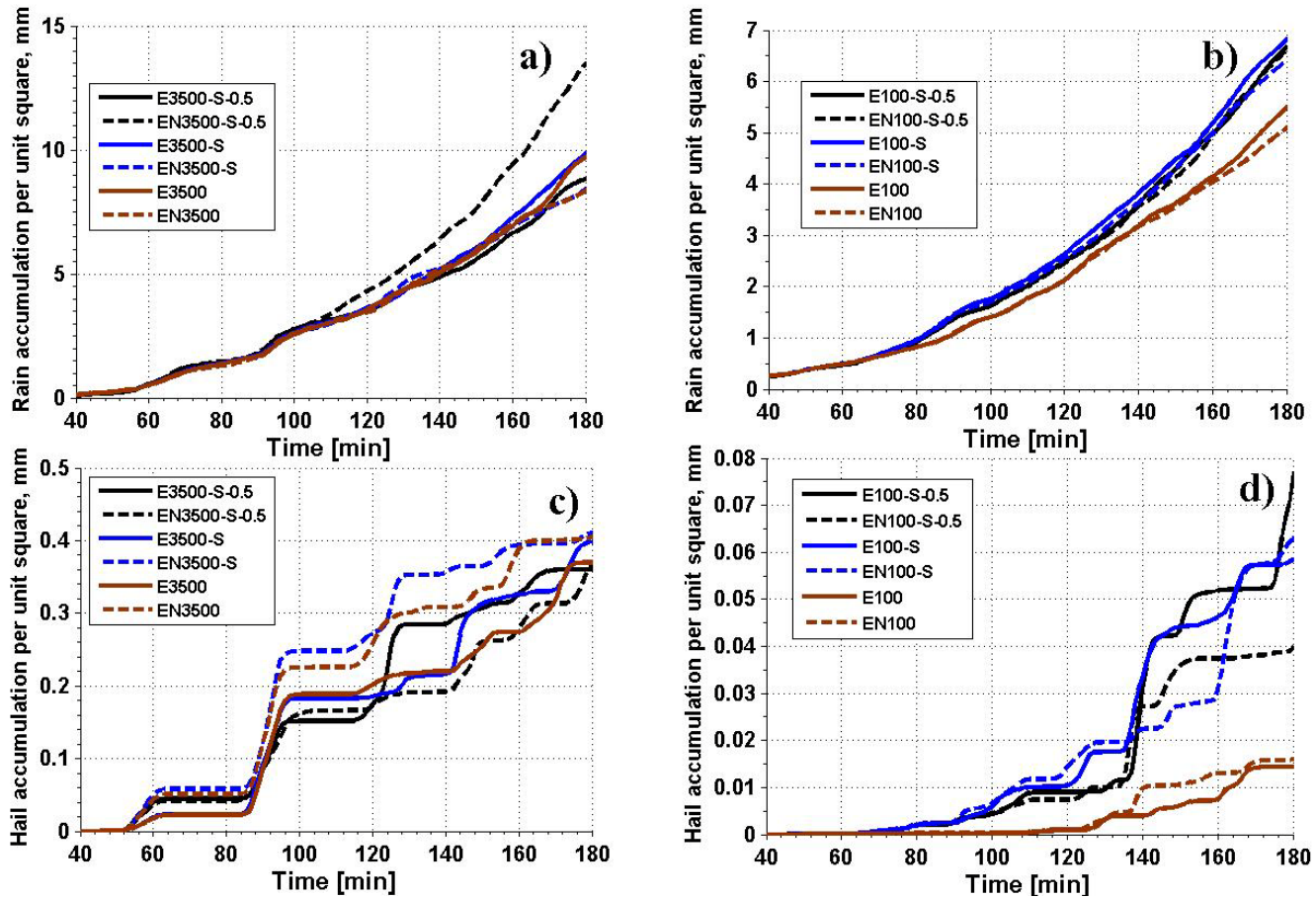
989

990

991

992

993



994

995

996

997 **Figure 10.** Time dependencies of (a) accumulated rain at surface for polluted and (b) for clean.
998 Accumulated hail at the surface for polluted (c) and for clean (d) in different simulations in
999 polluted cases.